Computer simulation of the characteristic curves of pure fluids

Ulrich K. Deiters[1]

Institute of Physical Chemistry, University of Cologne, Luxemburger Str. 116, D-50939 Köln, Germany

Arnold Neumaier

Department of Mathematics, University of Vienna, Oskar-Morgenstern-Platz 1, A-1090 Wien, Austria

[1]corresponding author, ulrich.deiters@uni-koeln.de

Abstract

Brown's characteristic curves (also known as ideal curves) describe states at which one thermodynamic property of a real pure fluid matches that of an ideal gas; these curves can be used for testing the extrapolation behaviour of equations of state. In this work, some characteristic curves are computed directly—without recourse to an equation of state—for some pair potentials by Monte Carlo computer simulation. The potentials used are an ab-initio potential for argon, the 1-center Lennard-Jones potential, and a softer pair potential whose short-range part is in accordance with quantum mechanical predictions. The influence of the short-distance repulsion on the characteristic curves is found to be significant even in the 10–100 MPa pressure range.

Keywords: Brown's characteristic curve; ideal curve; Monte Carlo simulation; pair potential; soft repulsion; Joule inversion; Joule–Thomson inversion

1 Introduction

An *ideal* gas is characterized by the conditions that its compression factor is 1 for all temperatures T and molar volumes V_m,

$$Z \equiv \frac{pV_\mathrm{m}}{RT} = 1 \ , \tag{1}$$

and that its configurational internal energy[2] is zero, $U = 0$. Consequently, the derivatives of Z with respect to volume or temperature are zero, too. For a *real* fluid, one or more conditions can be fulfilled for special V_m, T combinations only. In his article of 1960, Brown [1] notes that—as a consequence of Gibbs' phase rule—states of a pure real fluid for which one thermodynamic property matches that of an ideal gas can be represented by curves in the p, T plane. These curves, nowadays known as Brown's ideal curves or characteristic curves, can be computed with little effort for any equation of state and can be used as a first test of thermodynamic consistency and reasonable extrapolation behaviour [2, 3].

Brown's analysis is based on derivatives of the compression factor Z and therefore leads to the following characteristic curves:

0th order: There is one zeroth-order characteristic curve, namely the curve defined by Eq. (1). In the literature it is sometimes called the *ideal curve* or *Zeno curve*.

At high temperatures and low densities, in the limit $p \to 0$, the Zeno curve originates at the Boyle temperature T_B. From there is runs to lower temperatures, passing through a pressure maximum.

1st order: Brown defines three first-order characteristic curves:

[2] There may be other, non-configurational contributions to the internal energy which do not vanish. In this work we consider configurational properties only.

A: the *Amagat curve*, also known as Joule inversion curve. Its defining condition is any one of the following:

$$\left(\frac{\partial Z}{\partial T}\right)_V = 0 \quad \left(\frac{\partial U}{\partial V}\right)_T = 0 \quad \left(\frac{\partial p}{\partial T}\right)_V = \frac{p}{T} \tag{2}$$

Along the Amagat curve, the configurational internal energy of a fluid is independent of density. Usually $(\partial U/\partial V)_T$ of a fluid is negative: a compression forces the molecules into each other's potential wells, thus bringing about a negative contribution to internal energy. But at very high densities or at high collision speeds molecules may be driven into the repulsive branches of their interaction potentials, and then a positive contribution to internal energy results. At the Joule inversion points, the negative and the positive contributions cancel.

The Amagat curve starts at zero pressure at the temperature at which the second virial coefficient B_2 has its maximum. From there it runs through a pressure maximum to lower temperatures, until it ends (in a p,T projection) on the vapour pressure cuve—theoretically, for usually crystallization will occur before that endpoint.

The maximum of the Amagat curve is at very high pressures, typically 50–100 times the critical pressure. Therefore the Amagat curve is often ignored or regarded as "science fiction". This, however, would be a rash conclusion. For light gases like hydrogen, the Amagat curve lies at technically accessible pressures and temperatures; using an equation of state for hydrogen that cannot sensibly represent the Amagat curve would be a mistake. Moreover, the pressure range used in modern technologies is expanding all the time; e.g., nowadays natural oil and gas are sometimes produced from deep geological reservoirs having pressures above 100 MPa. It is advisable to describe their thermodynamic properties with equations of state that are reliable at such conditions.

B: the *Boyle curve*, which is defined by any one of

$$\left(\frac{\partial Z}{\partial V}\right)_T = 0 \quad \left(\frac{\partial Z}{\partial p}\right)_T = 0 \quad \left(\frac{\partial p}{\partial V}\right)_T = -\frac{p}{V}\,. \tag{3}$$

This curve originates on the temperature axis at the Boyle temperature the temperature for which $B_2 = 0$, passes through a pressure maximum, and ends on the vapour pressure curve (more precisely: on the liquid spinodal) close to the critical point.

C: the *Charles curve*, also known as Joule–Thomson inversion curve. It is defined by any one of

$$\left(\frac{\partial Z}{\partial T}\right)_p = 0 \quad \left(\frac{\partial Z}{\partial V}\right)_p = 0 \quad \left(\frac{\partial H}{\partial p}\right)_T = 0 \quad \left(\frac{\partial V}{\partial T}\right)_p = \frac{V}{T} \quad \left(\frac{\partial T}{\partial p}\right)_H = 0\,. \tag{4}$$

The Charles curve starts on the temperature axis at the temperature at which the slope of the second virial coefficient matches that of the secant, $\mathrm{d}B_2/\mathrm{d}T = B_2/T$. Like the Amagat and Boyle curves, it runs through a pressure maximum

to lower temperatures and ends on the vapour pressure curve. The Charles curve marks the transition from cooling to heating upon isenthalpic throttling and is therefore of paramount importance for gas liquefaction technology as well as for equipment safety.

Brown furthermore defines a number of second-order characteristic curves, but we shall not deal with them here.

From thermodynamic arguments together with physical plausibility considerations Brown deduces some general features of the characteristic curves. For example, the Amagat, Boyle, and Charles curves must not cross, but surround each other in a p, T diagram (Boyle inside Charles inside Amagat), as can be seen in Fig. 1, which shows these curves for the equation of state of the Lennard-Jones fluid by Mecke et al. [4, 5]. Another feature is that—in a double-logarithmic p, Tdiagram—the Amagat, Boyle, and Charles curves have negative curvatures everywhere (i.e., they are dome-shaped, with a single maximum and no inflection points), and their slopes tend to infinity for low pressures. These demands are not trivial. Fig. 2 compares the Amagat curves of several equations of state for the Lennard-Jones fluid. It turns out that only the equations of Mecke et al. [4, 5] and of Kolafa and Nezbeda [6] produce satisfactory Amagat curves (although the latter equation gives a spurious high-pressure branch at very low temperatures). The Amagat curve of the equation of Nicolas et al. [7] has positive slope (i.e., turns back) at high temperatures; the equation of Johnson et al. [8, 9] is distorted and interrupted. Moreover, the Amagat curves of the last two equations of state do not have the correct limit at high temperatures and low densities.

Thus Fig. 2 shows how Brown's characteristic curves may serve as a simple, but efficient test of the thermodynamic consistency and the extrapolation behaviour of equations of state.

On a second thought, however, Figs. 1 and 2 lead to some questions:

- The infinite slopes of the characteristic curves in the low-pressure limit are, of course, due to the logarithmic scaling. What are the "true" shapes of the characteristic curves, without the logarithmic distortions, and does Brown's postulate of negative curvature hold for linear scaling, too?[3]
- Do the characteristic curves in Fig. 1 represent the "real" behaviour of the Lennard-Jones fluid, or does the underlying equation of state cause distortions?

These questions can be answered by computing the characteristic curves directly—without making the detour of constructing and using an equation of state—by computer simulation.

This, however, immediately leads to the problem of the pair potential. Nowadays the Lennard-Jones pair potential is used in most thermodynamic simulations. But it is well known that it is "too hard", i.e., too repulsive at short distances. We will therefore also study the effect of a softer, more realistic repulsion on Brown's characteristic curves.

[3]It appears that few authors show the characteristic curves in non-logarithmic coordinates. Morsy [10] and Schaber [11] discuss the Zeno, Boyle, and Charles curves in (linear) p, T and ρ, T diagrams, but not the Amagat curves.

2 Computer simulations

2.1 Pair potentials

To determine the real shapes of the characteristic curves it is advisable to compute these *directly* by computer simulation. This avoids possible artifacts introduced by equations of state, and it permits studying the effect of the interaction potentials.

Particularly the behaviour of the Amagat curve is strongly affected by the details of the short-distance repulsive potential. Thus it is important to know its theoretical shape as predicted by quantum mechanics. The commonly used Lennard-Jones pair potential [12]

$$u(r) = 4\epsilon \left(\left(\frac{\sigma}{r}\right)^{12} - \left(\frac{\sigma}{r}\right)^{6} \right) , \tag{5}$$

where r denotes the center–center distance, σ the collision diameter, and ϵ the potential well depth, is a semiempirical potential. The r^{-6} factor in the attraction term can be explained by London's theory of dispersion interactions. The r^{-12} repulsion was found by Lennard-Jones to describe the virial coefficients of some simple gases well, but is mostly used because of computational convenience. From Hugoniot curves, gas viscosities, and other experiments sensitive to intermolecular repulsion it is known that the Lennard-Jones potential is "too hard" at short distances.

The repulsion between two neutral molecules is a quantum mechanical phenomenon. One of the earliest attempt to derive a more realistic pair potential from quantum mechanic principles was that of Buckingham [13]. The so-called Buckingham pair potential

$$u(r) = a_1 e^{-\alpha r} - \frac{a_2}{r^6} , \tag{6}$$

where a_1, a_2, and α are substance-dependent parameters, is not only frequently used in computer simulations, but became the "ancestor" of many other, more sophisticated pair potentials, which were derived from it by adding additional terms for Coulomb interactions or higher-order dispersion forces. The drawback of the Buckingham potential is that it runs to $-\infty$ for $r \to 0$, i.e., it becomes infinitely attractive. Therefore it has to be replaced by another pair potential at short distances, and we do not consider it in this work.

Pathak and Thakkar [14] state that united-atom perturbation theory implies

$$u(r) = a_1 \frac{z^2}{r} + a_2 + O(r^2) \quad \text{for } r \ll r_\mathrm{e} \tag{7}$$

for monoatomic gases. Here z is the nuclear charge, r_e the equilibrium distance, a_1 a universal parameter ($a_1 = 1$ in Hartree atomic units), and a_2 a substance-dependent parameter. Incorporating exchange effects that lead to exponential screening of the Coulomb potential [15] leads to

$$u(r) = e^{-\alpha r} \left(a_1 \frac{z^2}{r} \left(1 - \frac{(\alpha r)^2}{2} \right) + a_2 (1 + \alpha r) \right) \quad \text{for } r \ll r_\mathrm{e} . \tag{8}$$

Therefore empirical pair potentials merely fitted to data at larger r should be modified such that they have the correct short-distance behavior Eq. (8). This can be done by matching a_2 and α to the value $u_\mathrm{s} = u(r_\mathrm{s})$ and the slope $u'_\mathrm{s} = u'(r_\mathrm{s})$ of the potential at a suitably small switching radius r_s. One can easily verify that

$$\alpha^2 r u(r) + (1 + \alpha r) u'(r) = e^{-\alpha r} a_1 \frac{z^2}{2r^2} (1 + \alpha r)(2 + 2\alpha r + 3(\alpha r)^2 - (\alpha r)^3 - (\alpha r)^4) , \tag{9}$$

which, evaluated at r_s, gives a nonlinear equation to be solved for α; then a_2 can be found from the equation for $u(r)$. Varying r_s gives different variants of the same potential, and can be used—if the limiting behavior of the empirical potential is different from Eq. (8)—to assess the effect of the very repulsive part of the potential.

A similar correction was made by Vogel et al. [16–18] for an otherwise very accurate ab-initio potential for argon. They use $r_\mathrm{s} = 0.4 r_\mathrm{e}$, but match the constants a_1 and α of the theoretically less adequate asymptotic repulsive potential $a_1 e^{-\alpha r}/r$ to u_s and u'_s.

The helium pair potential of Jeziorska et al. [19] respects the asymptotic relation Eq. (7) and therefore does not need such a switchover.

In order to allow a better comparison with the Lennard-Jones potential, the pair potential

$$u(r) = a_1 e^{-2\alpha r} \left(\alpha + \frac{1}{r}\right) - \frac{a_2 r^2}{a_3 + r^8} \tag{10}$$

with positive parameters α, a_1, …,a_3 is used in this work. This function exhibits the theoretically correct r^{-6} behaviour at large distances, the desired short-range behaviour according to Eq. (8), and avoids the negative (i.e., infinitely attractive) pole at $r = 0$.

For our simulations the parameters of this pair potential were chosen in such a way that the locations of the zero and the potential minimum as well as the curvature at the minimum match those of the Lennard-Jones potential[4]. The resulting values of the parameters are shown in Tab. 1.

Fig. 3 compares this pair potential and the Lennard-Jones potential at small and intermediate distances. It turns out that the two potentials are practically indistinguishable in the region of the potential well, but that the new potential is "softer" at small distances, as demanded by theory.

The ab-initio pair potential of Vogel et al. is shown in this diagram, too. That it deviates from the other two potential functions is not surprising: The potential function of Vogel et al. is a *true* pair potential function, whereas the other two are *effective* potential functions, optimized for the liquid state at moderate pressures.

Fig. 4 shows the second virial coefficients computed for the Lennard-Jones potential and Eq. (10) by numerical integration. The curves are almost indistinguishable. An inspection of the numerical results shows that the second virial coefficient of the new pair potential is larger by 9.6 cm^3/mol at 50 K (where B_2^LJ amounts to –626.7 cm^3/mol) and 0.26 cm^3/mol at 10000 K (where B_2^LJ amounts to +23.74 cm^3/mol).

2.2 Simulation details

The characteristic curves for the pair potentials listed above were determined from Monte Carlo simulations, using our own program mc++ [20]. The simulations were performed for isobaric–isothermal ensembles of 1000 particles, using a cubic simulation box, periodic boundary conditions, and a fast version of the minimum image convention [21]. For all simulations a potential cut-off distance of 4σ was used, and the usual spherical tail corrections to the thermodynamic functions were applied.

The simulation ensembles were assembled by placing the molecules randomly into a very large simulation box, which was then compressed until the desired pressure was reached. The ensembles were equilibrated for 10–20000 cycles, with a cycle consisting of 1000 attempted

[4] Maple® code for this is given in the Supplement

molecule displacements and one volume fluctuation. The production phase of the simulation consisted of 240000 cycles. A particular feature of the mc++ code is that, after the equilibration phase, the simulation is carried out in several parallel threads, so that it is possible to monitor the loss of spatial correlation with time and to ensure the statistical independence of the results.

In typical simulation runs for fluid states, the threads converge—within statistical uncertaincies—to the same results. Furthermore, the mean squared displacement per cycle should be approximately the same for all threads, and it should be large enough to indicate structural randomization. For example, a value of 0.003 Å^2, as found for the rather extreme case of 80 K and 20 MPa, means that an argon atom has traveled about 15.5 Å (4.5 collision diameters) from its original position during a thread duration of 80000 cycles. This clearly indicates a fluid state, whereas traveling distances less than a collision diameter and disagreeing thread results would indicate at least an insufficient thread length and, most likely, a partial crystallization.

Compression factors $Z = pV_\mathrm{m}/(RT)$ were determined from the (given) pressure and the molar volumes as well as from evaluating the virial. Except for the critical region, where the deviations were slightly larger, the results usually agreed within 0.05%.

The characteristic curves were determined from the simulation results as follows:

1. Amagat curve: The residual molar energy U_m^r was plotted against pressure at constant temperature. The minima, which indicate the Joule inversion, were obtained by parabolic approximation.
2. Boyle curve: The compression factor Z was plotted against pressure at constant temperature, and the minima were obtained by parabolic approximation.
3. Charles curve: The residual molar enthalpy H_m^r was plotted against pressure at constant temperature. The minima, which indicate the Joule–Thomson inversion, were obtained by parabolic approximation.
4. Zeno curve: The compression factor Z was plotted against pressure at constant temperature, and the pressure belonging to $Z = 1$ was obtained by parabolic approximation. Near the low-temperature endpoint of this curve, which is rather close to the critical point, cubic-spline interpolation was used.

In each case, the parabolic approximations were made with at least five points to ensure numeric stability.

2.3 Simulation results: Amagat curve

Fig. 5 shows the residual internal energy[5] of the Lennard-Jones fluid, as determined by Monte Carlo simulation, as a function of pressure. The Joule inversion points correspond to minima of the isotherms. It turns out that the equation of state by Mecke et al. [4, 5] predicts the Joule inversion of the Lennard-Jones fluid remarkably well.

At high pressures and temperatures below 150 K, the simulation ensembles show signs of crystallization. Then the localization of the minima by parabolic approximation becomes unreliable or even impossible.

At a first glance, the energy–pressure diagrams for the argon ab-initio potential (Fig. 6) and the Eq. (10) potential (Fig. 7) look very similar. Differences become apparent in the pressure–temperature diagram, Fig. 8: The ab-initio potential, being a true two-body potential, yields

[5]Tables containing the simulation results can be found in the Supplement.

a rather different Amagat curve. The Amagat curves of the Lennard-Jones and the Eq. (10) potential almost coincide up to 1000 K. For higher temperatures, the curve of the Lennard-Jones potential is slightly higher. In this temperature range, the Amagat curve of the Eq. (10) potential has a slight positive curvature.

At high temperatures, the Amagat curves end on the abscissa at temperatures at which the 2nd virial coefficient $B_2(T)$ has a maximum. These endpoints were determined by numerically computing second virial coefficients for the potentials considered here.

The positive curvature is discernible in a linearly scaled p, T diagram; it does not exist in the logarithmic representation. Moreover, we note that the Amagat curves are not dome-shaped in a linearly scaled diagram, but rather unsymmetric (shark-fin-shaped).

2.4 Simulation results: Charles and Zeno curves

Figs. 10 and 11 show residual enthalpy isotherms, from which the Joule–Thomson transition can be determined. Again, the equation of state of Mecke et al. [4, 5] matches the simulation results for the Lennard-Jones potential very well.

Figs. 12 and 13 compare the Charles and Zeno curves obtained for the pair potential Eq. (10) and the Lennard-Jones potential. The results agree qualitatively; all the curves have a single pressure maximum and no inflection points. But it is remarkable that the results for the two pair potentials differ significantly, although the pair potentials differ in the short-distance repulsive part only.

2.5 Simulation results: Boyle curve

The Boyle curve extends to moderately high densities only. Even here, however the curves for the Lennard-Jones potential and Eq. (10) differ, as can be seen in Fig. 14. The results for high temperatures shown in this diagram are less precise, however, for here the fluid is almost an ideal gas, and the deviations from ideality—which are responsible for the existence of the Boyle curve—can be obtained with a large statistical uncertainty only.

3 Conclusion

In this work, Brown's zeroth-order and first-order characteristc curves—the Amagat (Joule inversion), Boyle, Charles (Joule–Thomson inversion), and Zeno curve (ideal) curve—were computed directly by Monte Carlo computer simulation. The simulations were carried out for two different pair potentials, namely the well-known Lennard Jones potential (with the common interaction parameters for argon) and a newly developed pair potential with an exponential repulsion term. The new pair potential closely matches the Lennard-Jones potential function for distances in the range of the attractive potential well, but is less repulsive ("softer") at short distances; its limiting behaviour for $r \to 0$ agrees with quantum mechanical predictions.

In addition, simulations were carried out with the argon ab-initio pair potential of Vogel et al. [16–18] for the Amagat curve, which runs to very high pressures.

The characteristic curves for the Lennard-Jones fluid obtained by Monte Carlo simulation agree remarkably well with the curves obtained from the equation of state of Mecke et al. [4, 5]. The equation of state of Kolafa and Nezbeda [6] describes the Lennard-Jones fluid well, too, but its Amagat curve exhibits an artifact at high pressures and low temperatures. The equation of

Johnson et al. [8,9] and its predecessor, the equation of Nicolas et al. [7] have distorted Amagat curves.

For the simple, nonpolar model fluid studied in this work, Brown's postulates

1. that the Amagat, Boyle, and Charles curves do not intersect,
2. that the Amagat curve surrounds the Charles curve, and the latter the Boyle curve,
3. that the Zeno curve intersects the Amagat and Boyle curves once,
4. and that these curves, in a double-logarithmic p, T diagram, have a dome shape with a negative curvature everywhere

could all be confirmed.[6]

In a linear-scale p, T diagram, however, the characteristic curves look rather unsymmetric ("shark-fin shape"). The Amagat curve of the new, soft pair potential has a region of positive curvature at high temperatures.

Although the Charles and Zeno curves lie at much lower pressures than the Amagat curve, these two curves show a significant effect of the softness of the pair potential. E.g., in our simulations of argon, the Charles curves differ by about 1.8 MPa at 55 MPa, and the residual enthalpies by almost 100 J/mol, which corresponds to almost 5%. The Boyle curves differ, too, but here the precision of the simulation is not as high as for the other curves, for Z is usually obtained with a larger statistical error than U_m or H_m. This means that the characteristic curves—and some thermodynamic properties related to them—are more sensitive to the shape of the repulsive part of the pair potential than is usually assumed.

Conversely one may conclude that the pair potential proposed in this work is preferable over the Lennard-Jones potential for computer simulations at elevated pressures.

Acknowledgments

The authors thank the computing center of the University of Cologne (RRZK) for providing CPU time on the CHEOPS supercomputer (funded by Deutsche Forschungsgemeinschaft) as well as for technical support.

Symbols

a_i	pair potential parameter, $i = 1, 2, \ldots$
B_i	ith virial coefficient
H	configurational enthalpy
k_B	Boltzmann's constant
p	pressure
R	universal gas constant
r	intermolecular distance

[6] A study of the characteristic curves of water, a strongly polar fluid, is underway.

T	temperature
U	configurational internal energy
u	intermolecular pair potential
V	volume
Z	compression factor, $Z = pV_\mathrm{m}/(RT)$
z	nuclear charge number
α	pair potential parameter (charge screening)
ϵ	energy parameter of the Lennard-Jones potential
σ	size parameter of the Lennard-Jones potential

Subscripts

e	equilibrium value
m	molar property
s	pair potential switchover

References

[1] Brown, E. H. *Bull. Intnl. Inst. Refrig., Paris, Annexe* **1960**, *1960-1961*, 169–178.

[2] Span, R.; Wagner, W. *Int. J. Thermophys.* **1997**, *18*, 1415–1443.

[3] Deiters, U. K.; de Reuck, K. M. *Pure Appl. Chem.* **1997**, *69*, 1237–1249.

[4] Mecke, M.; Müller, A.; Winkelmann, J.; Vrabec, J.; Fischer, J.; Span, R.; Wagner, W. *Int. J. Thermophys.* **1996**, *17*, 391–404.

[5] Mecke, M.; Müller, A.; Winkelmann, J.; Vrabec, J.; Fischer, J.; Span, R.; Wagner, W. *Int. J. Thermophys.* **1998**, *19*, 1493.

[6] Kolafa, J.; Nezbeda, I. *Fluid Phase Equilib.* **1994**, *100*, 1–34.

[7] Nicolas, J. J.; Gubbins, K. E.; Streett, W. B.; Tildesley, D. J. *Mol. Phys.* **1979**, *37*, 1429–1454.

[8] Johnson, J. K.; Zollweg, J. A.; Gubbins, K. E. *Mol. Phys.* **1993**, *78*, 591–618.

[9] Johnson, J. K.; Müller, E. A.; Gubbins, K. E. *J. Phys. Chem.* **1994**, *98*, 6413–6419.

[10] Morsy, T. E.; Ph.D. thesis; Technische Hochschule Karlsruhe, Germany; 1963.

[11] Schaber, A.; Ph.D. thesis; Technische Hochschule Karlsruhe, Germany; 1965.

[12] Lennard-Jones, J. E. *Proc. Royal Soc. London A* **1924**, *106*, 463–477.

[13] Buckingham, R. A. *Proc. Royal Soc. London Ser. A* **1938**, *168*, 264–283.

[14] Pathak, R. K.; Thakkar, A. J. *J. Chem. Phys.* **1987**, *87*, 2186–2190.

[15] Buckingham, R. A. *Trans. Faraday Soc.* **1958**, *54*, 423–459.

[16] Jäger, B.; Hellmann, R.; Bich, E.; Vogel, E. *Mol. Phys.* **2009**, *107*, 2181–2188.

[17] Jäger, B.; Hellmann, R.; Bich, E.; Vogel, E. *Mol. Phys.* **2010**, *108*, 105.

[18] Vogel, E.; Jäger, B.; Hellmann, R.; Bich, E. *Mol. Phys.* **2010**, *108*, 3335–3352.

[19] Jeziorska, M.; Cencek, W.; Patkowski, K.; Jeziorski, B.; Szalewicz, K. *J. Chem. Phys.* **2007**, *127*, 124303.

[20] Deiters, U. K.; mc++ project homepage: http://www.uni-koeln.de/deiters/mc++/index.html.

[21] Deiters, U. K. *Z. Phys. Chem.* **2013**, *227*, 345–352.

[22] Deiters, U. K.; *ThermoC* project homepage: http://thermoc.uni-koeln.de/index.html.

Appendix 1 Tables

Table 1: Pair potential parameters for argon.

parameter	Ar
Lennard-Jones	
ϵ/k_{B}	119.8
$\sigma/\mathring{A}$	3.405
Eq. (10)	
$a_1/(\mathrm{K\,\mathring{A}})$	1.639146038×10^9
$\alpha/\mathring{\mathrm{A}}^{-1}$	2.503350833
$a_2/(\mathrm{K\,\mathring{A}}^6)$	7.075527590×10^5
$a_3/\mathring{\mathrm{A}}^8$	2.726770354×10^4

Appendix 2 Figures

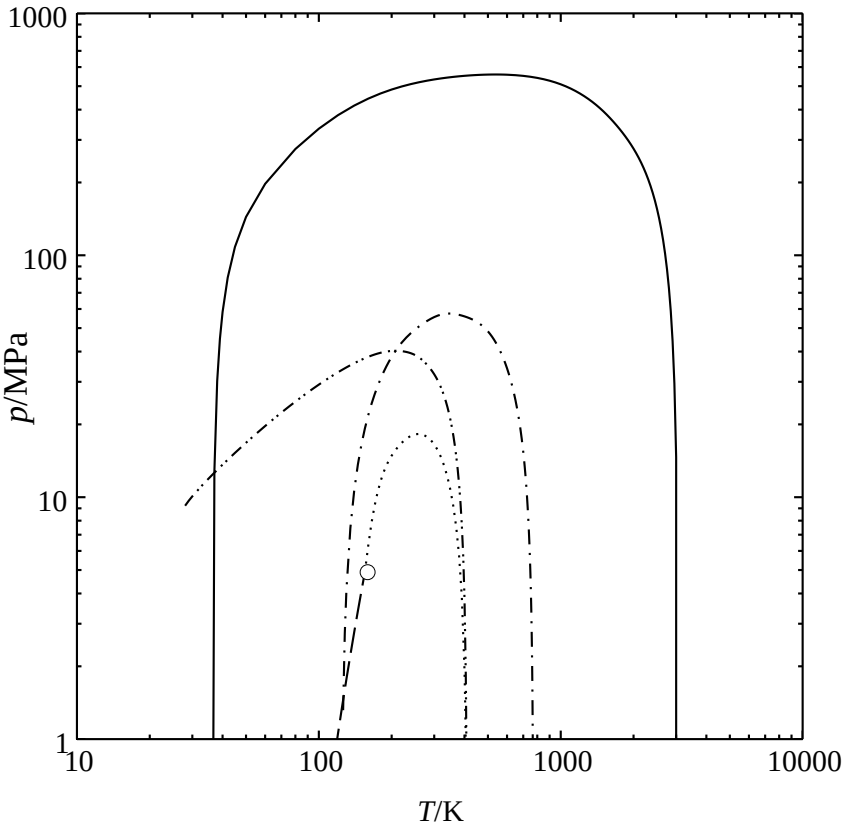

Fig. 1: Brown's characteristic curves for the equation of state of the Lennard-Jones fluid by Mecke et al. (parameters of argon), double-logarithmic representation. – – : vapour pressure curve, ○: critical point, ——: Amagat curve, · · · · · · : Boyle curve, –·– : Charles curve, –··– : Zeno curve. The curves were computed with the *ThermoC* program package [22].

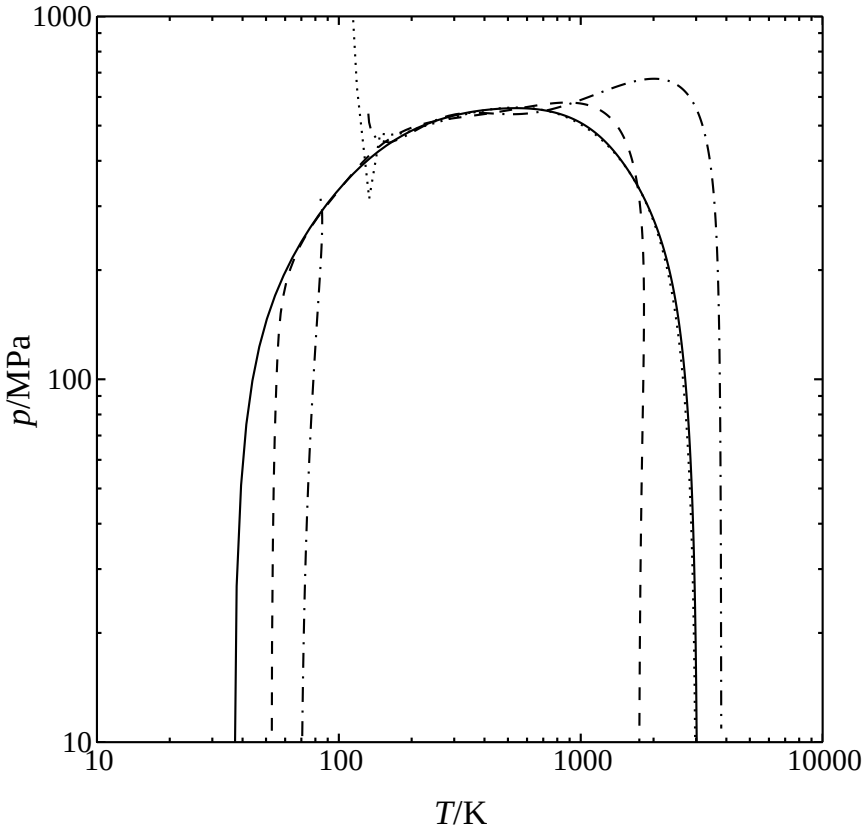

Fig. 2: Amagat curves for several equations of state for the Lennard-Jones fluid (parameters of argon). ——: Mecke et al., ·····: Kolafa and Nezbeda, - - - -: Nicolas et al., –·– : and Johnson et al.

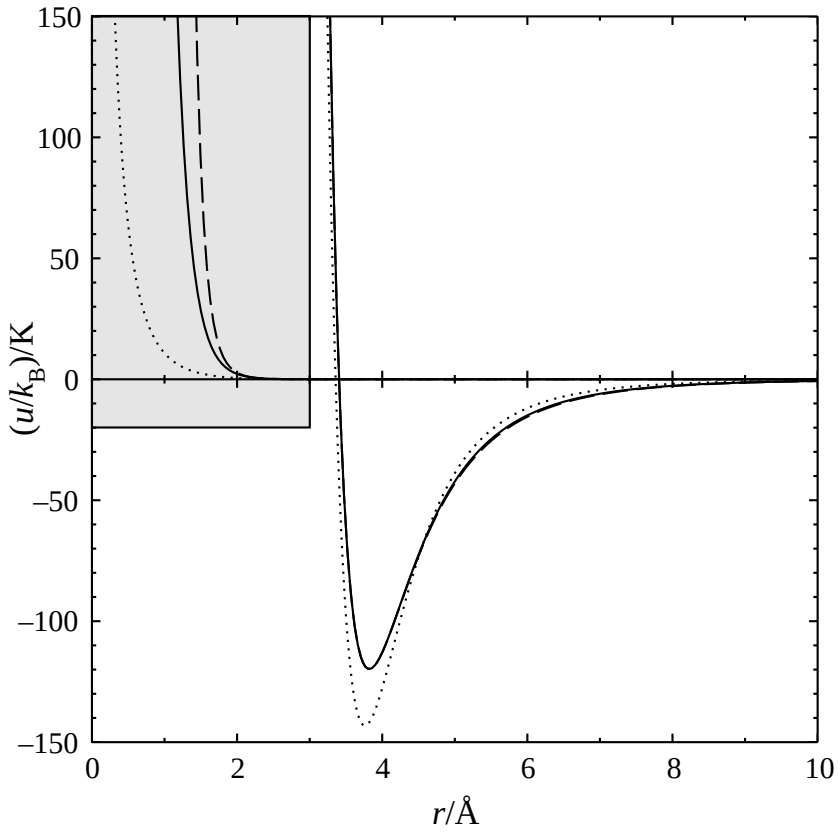

Fig. 3: Pair potential functions of argon. ——: Eq. (10), ·····: ab-initio pair potential of Vogel et al., – – : Lennard-Jones potential. Insert: behaviour of the potential functions at small distances (energies scaled by 10^{-5}).

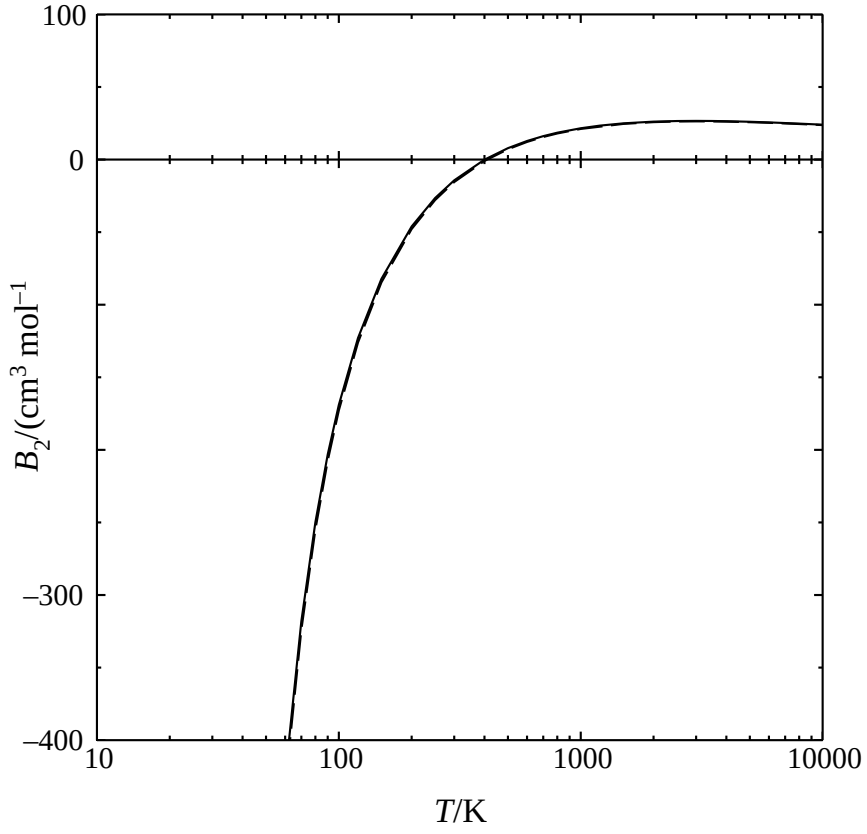

Fig. 4: The second virial coefficient as a function of temperature for different pair potentials. ——: Eq. (10), – – : Lennard-Jones potential.

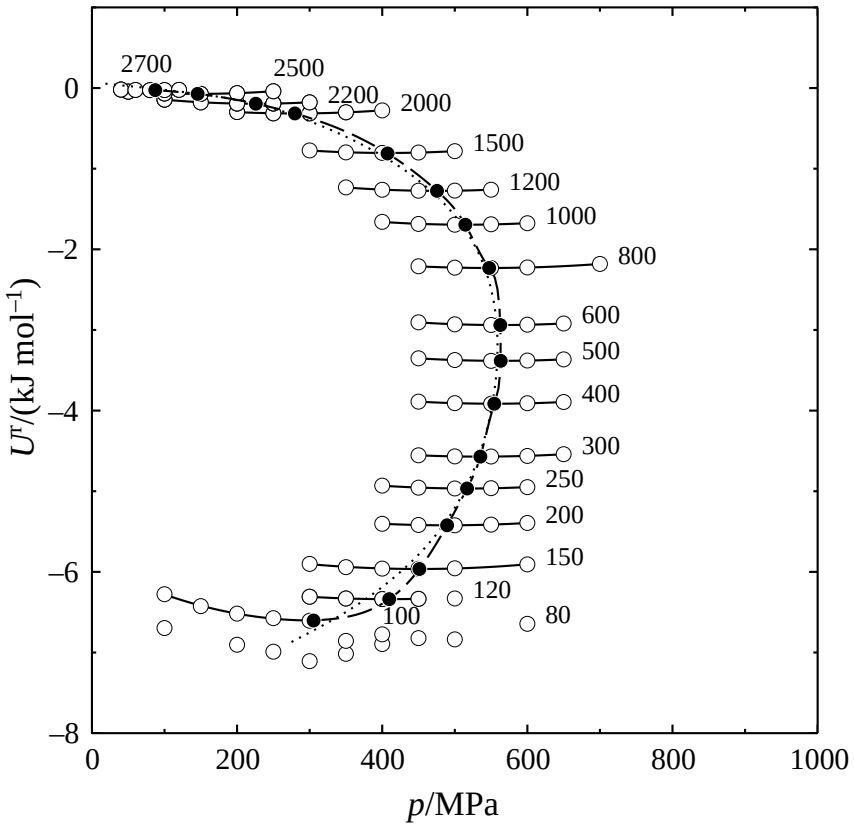

Fig. 5: Joule inversion I: The residual internal energy as a function of pressure for Lennard-Jones argon. Parameter: T/K. ○: simulation results, ——: approximation parabolas, ○: their minima, – – : interpolation curve through them, ·····: equation of state by Mecke et al.

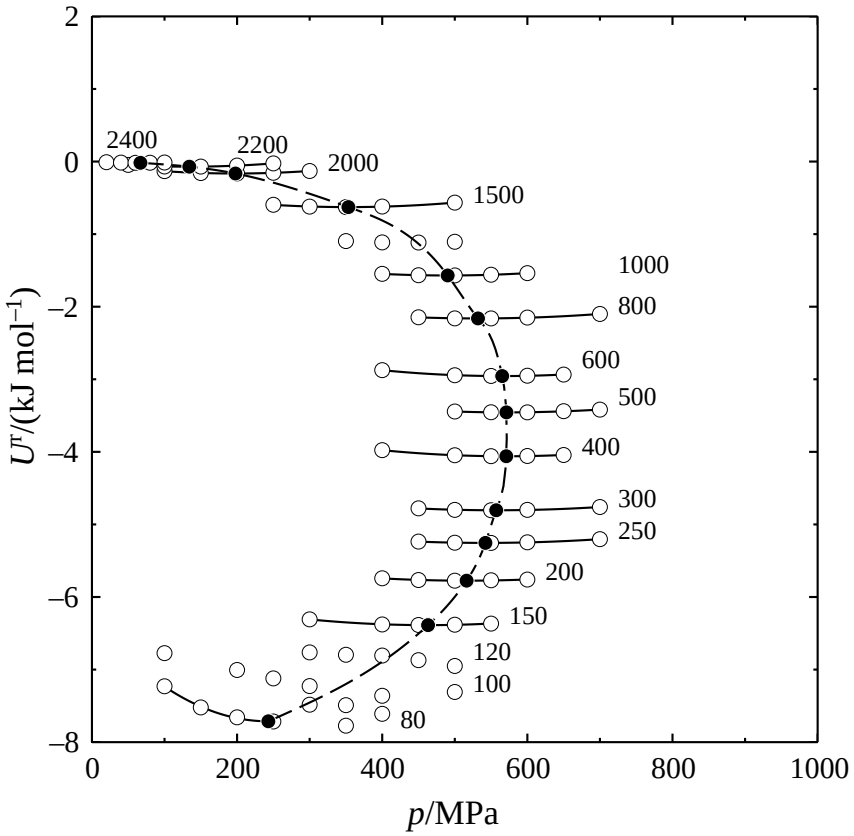

Fig. 6: Joule inversion II: The residual internal energy as a function of pressure, using the argon ab-initio potential of Vogel et al. For an explanation of the symbols and curves see Fig. 5; the highest temperatures in this diagram are 2200 and 2400 K.

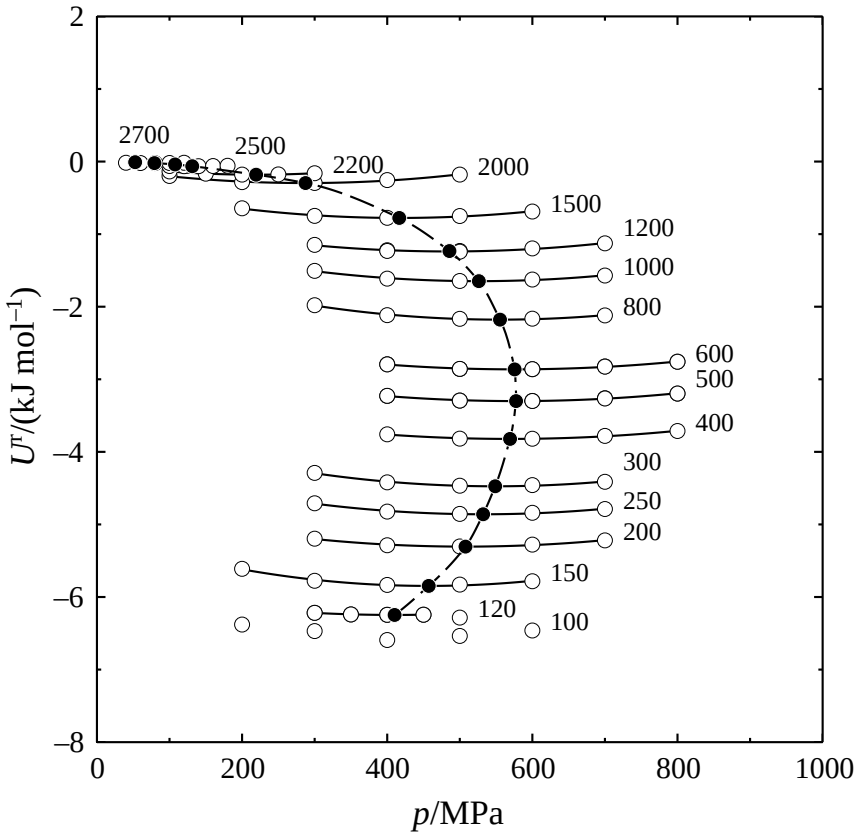

Fig. 7: Joule inversion III: The residual internal energy as a function of pressure, using the argon Eq. (10) potential. For an explanation of the symbols and curves see Fig. 5.

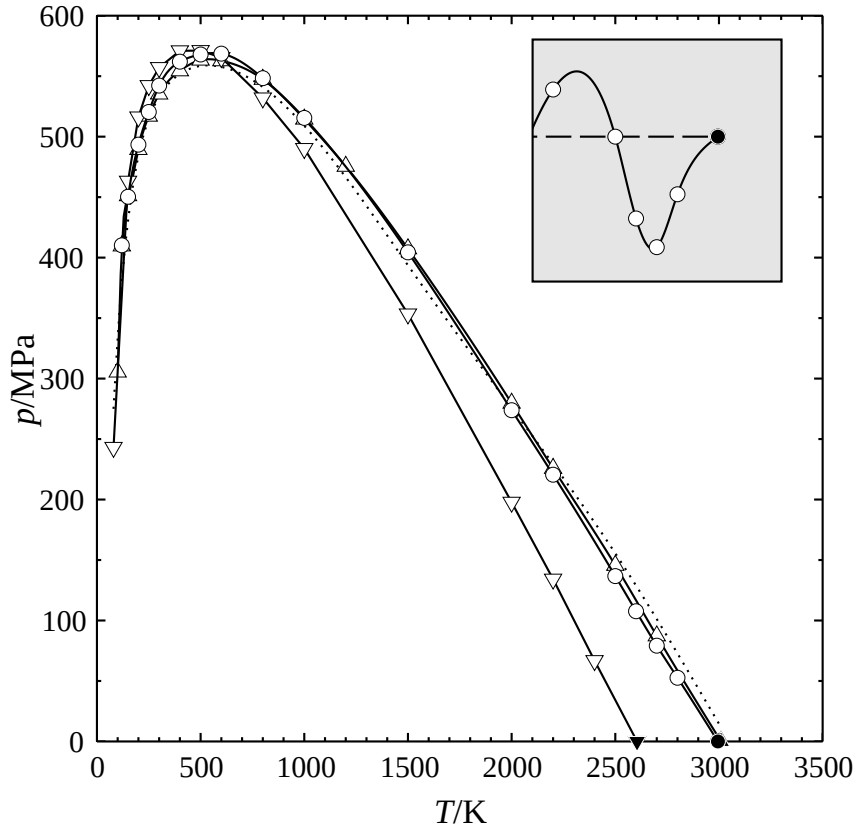

Fig. 8: Amagat curves (Joule inversion curves) of argon, calculated for various pair potentials. Open symbols: computer simulation (this work): ○: computer simulation (this work): △: Lennard-Jones, ○: Eq. (10), ∇: Vogel et al. ab-initio; filled symbols: maximum of the 2nd virial coefficient (numerical integration); · · · : equation of state of Mecke et al. [4,5], ——: interpolation function serving to guide the eye. Insert: difference of Eq. (10) Amagat curve and linear interpolation (– –) between the first and the 2500 K data point, shown in order to prove that the curvature of the Amagat curve is positive at high temperatures.

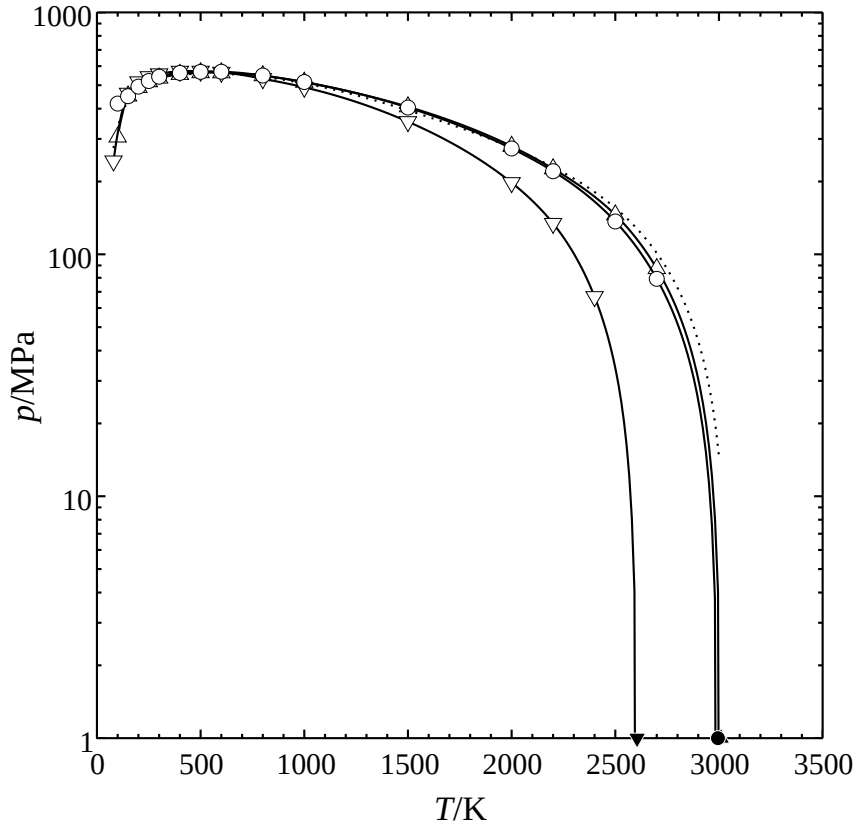

Fig. 9: Amagat (Joule inversion) curves of argon, calculated for various pair potentials—semilogarithmic representation. See Fig. 8 for an explanation of the symbols and curves.

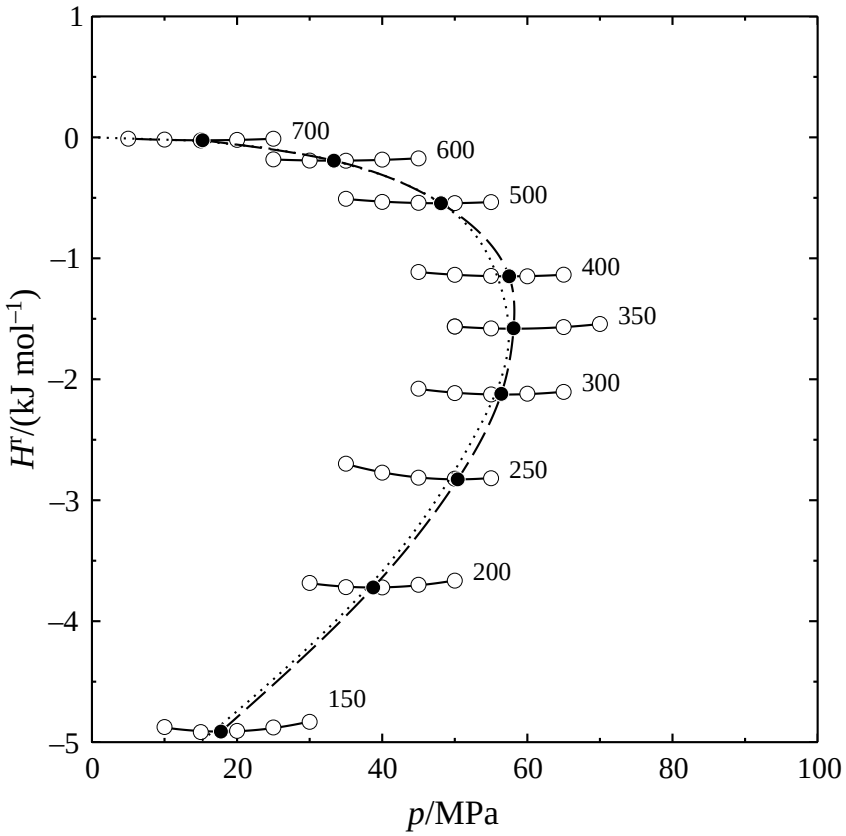

Fig. 10: Joule–Thomson inversion I: The residual enthalpy as a function of pressure for Lennard-Jones argon. Parameter: T/K. ○: simulation results, ——: approximation parabolas, ●: their minima, – – : interpolation curve through them, ·····: equation of state by Mecke et al.

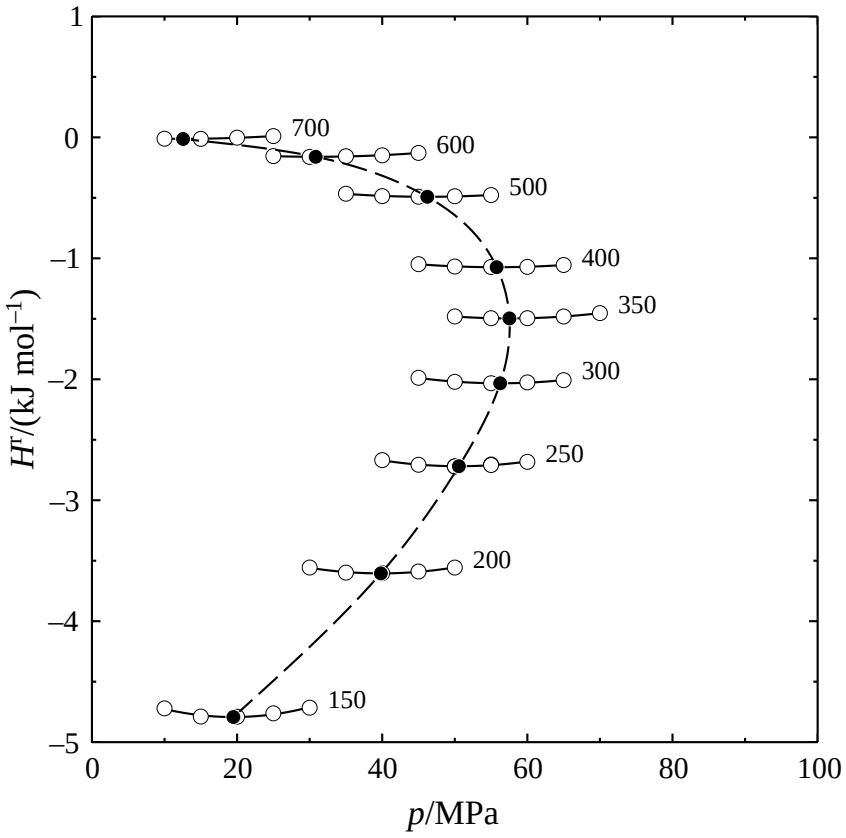

Fig. 11: Joule–Thomson inversion II: The residual enthalpy as a function of pressure, using the argon Eq. (10) potential. For an explanation of the symbols and curves see Fig. 10.

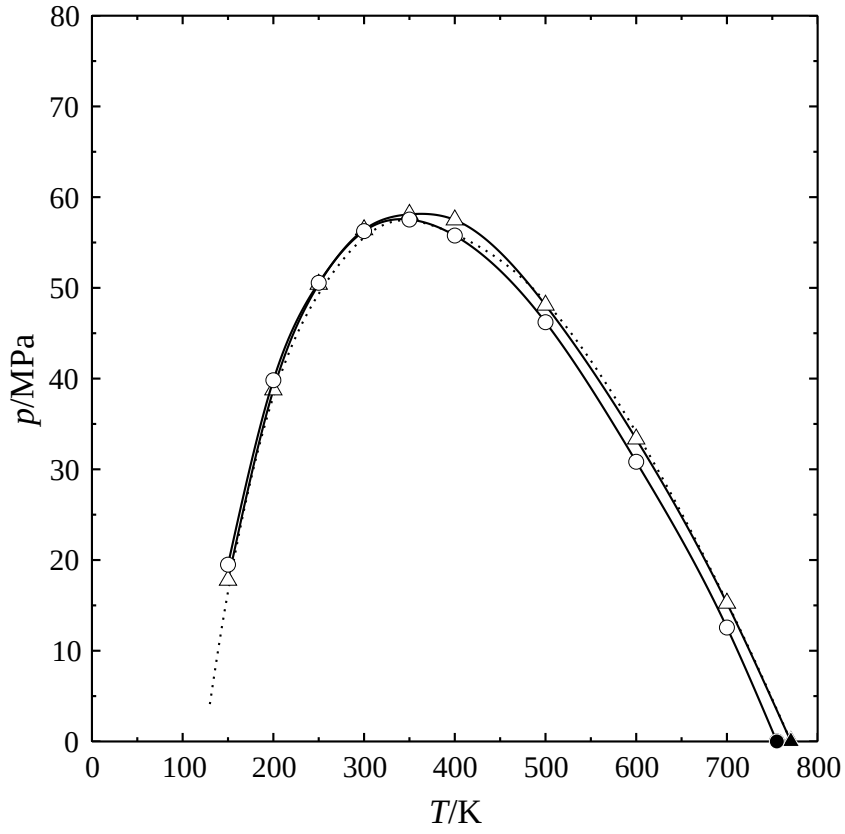

Fig. 12: Charles (Joule–Thomson inversion) curves of argon, calculated for various pair potentials. Open symbols: computer simulation (this work): ○: computer simulation (this work): △: Lennard-Jones, ○: Eq. (10); filled symbols: low-pressure limit calculated from the 2nd virial coefficient (numerical integration); · · ·: equation of state of Mecke et al., ——: interpolation function serving to guide the eye.

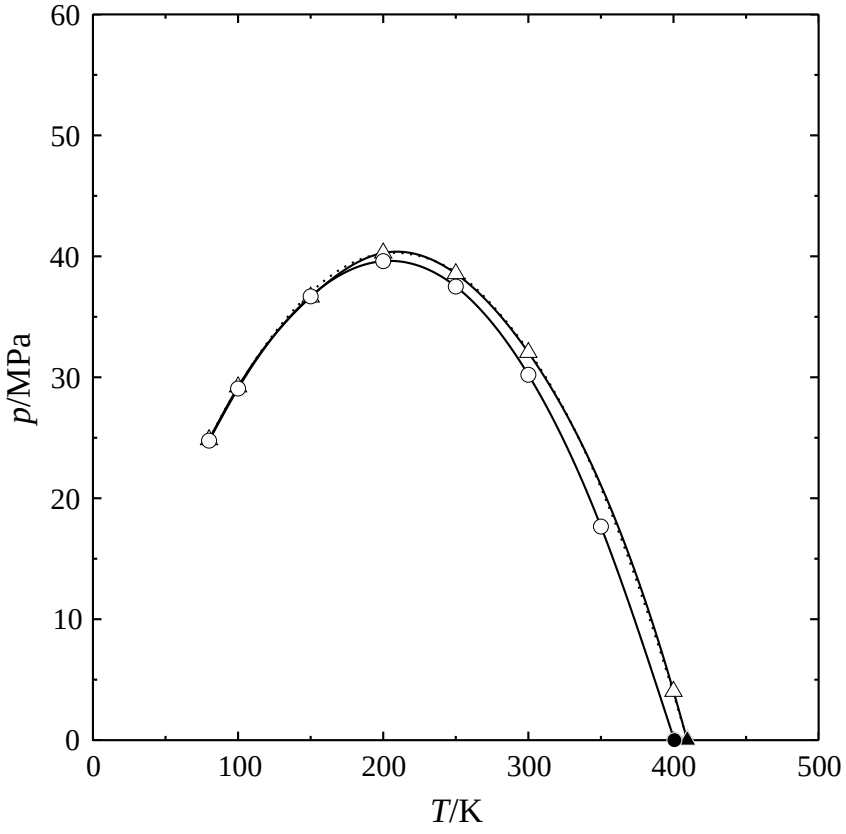

Fig. 13: Zeno ($Z = 1$) curves of argon, calculated for various pair potentials. See Fig. 12 for an explanation of the symbols.

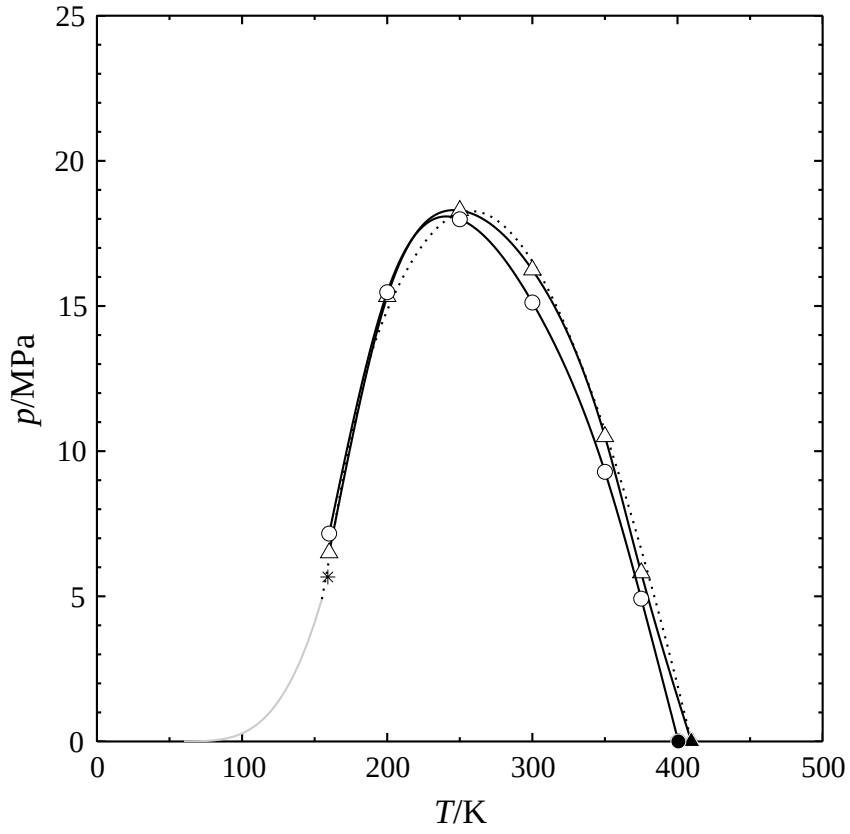

Fig. 14: Boyle curves of argon, calculated for various pair potentials. Open symbols: computer simulation (this work): ○: computer simulation (this work): △ Lennard-Jones, ○: Eq. (10); filled symbols: Boyle temperature calculated from the 2nd virial coefficient (numerical integration); · · · : equation of state of Mecke et al. [4, 5], ——: interpolation function serving to guide the eye; grey curve: vapour pressure curve, ∗: critical point.